Boundary Layer Transition, Separation and Flow Control on Airfoils, Wings and Bodies in Numerical, Wind-Tunnel and In-Flight Studies

Lukas Popelka
Institute of Thermomechanics, Academy of Sciences of the Czech Republic, Prague
popelka@it.cas.cz

Milan Matejka
Faculty of Mechanical Engineering, Czech Technical University in Prague
milan.matejka@fs.cvut.cz

David Simurda and Natalie Souckova
Institute of Thermomechanics, Academy of Sciences of the Czech Republic, Prague
simurda@it.cas.cz, natalies@it.cas.cz

Abstract

Particle Image Velocimetry (PIV), smoke-wire, tuft filaments and oil-flow visualization techniques were used for wind-tunnel and in-flight investigations of boundary layer separation, both stall and separation bubbles, related to the low-Reynolds number transition mechanism. Airfoils of three Czech-designed sailplanes and their wing-fuselage interaction were studied. The combination of experimental results with those of numerical modeling (computational fluid dynamics, CFD) greatly facilitated the understanding of the various phenomena. The effects of several passive flow control devices, vortex generators, counter-rotating vortex generators, and zig-zag type turbulators were considered. Separation suppression was reached and corresponding drag coefficient reduction occurred for test aircraft measured in flight. Investigations were extended by the PIV time-resolved technique.

Nomenclature

c_p	pressure coefficient	-
c	chord length	m
L/D	glide ratio (lift/drag)	-
q	dynamic pressure	Pa
Re	Reynolds number	-
Tu	intensity of turbulence	-
v	velocity magnitude	m/s
V (IAS)	airspeed (indicated)	km/h
Axis		
x	Longitudinal	
z	Spanwise	
Greek symbols		
α	angle of attack	deg
γ	flap angular deflection	deg
Π	normalized pressure difference	-
Subscripts		
b	bottom side	
t	top side	
T	Turbulator	

Introduction

The typical configuration of sailplanes has been fixed for many years and thoroughly investigated[1]. Still, the combination of all available analysis methods can bring better understanding to the flowfield aerodynamics and, consequently, to improvements in the design process. Likewise, as the quest for performance leads to further extensions of laminar flow and larger flap deflections, new phenomena are appearing, such as laminar and turbulent separation on control surfaces.

Passive flow control devices supply momentum to the boundary layer in the vicinity of sailplane surfaces; they can speed up the transition process in order to prevent laminar separation and/or to suppress turbulent separation. Although the passive flow control devices often show detrimental performance in off-design conditions, their simple application and reliability in service still make them worthwhile.

Boundary-layer development on wing and empennage airfoils, on wings with winglets and on the entire configuration was investigated. The understanding gained has been used for both the improvement of sailplanes in service, as well as for those still in development.

Geometries subject to study

The primary and applied research was coupled with three Czech designed and manufactured sailplanes (Figs. 1 and 2). The VSO10 is the most widely used single-seat sailplane in the Czech Republic (CR). The TST10 is a new microlight sailplane with self-launching ability aimed at leisure flying and club class handicapped competition. Lastly, the HPH304S is a new 18m FAI class racing sailplane that is optionally available with a self-launching piston engine, or jet-engine sustainer. For an additional comparison, the latest generation club class

sailplane, the HPH304C, was added to the research effort (Fig. 1).

The VSO10 test program employed an outer wing segment whose dimensions were suitable for wind-tunnel testing. The section used a linear transition from the Wortmann FX60-126 airfoil to the FX61-163 airfoil.[2] The tip geometry was the FX60-126 with a 25% chord aileron. To enable comparisons, the wingtip with aileron was built in the negative moulds of HPH304C sailplane. For wing-fuselage the interaction study, a VSO10C sailplane, call-sign OK-0530, was used.

The TST10 research program was initiated by in-flight measurements on a particular self-launching TST-10a sailplane, call sign OK-A631. The fuselage shape followed published coordinates[3] (Model No. 1) and, together with a Wortmann FX66-series wing airfoil,[2] created a suitable test case for the wing/fuselage interaction investigation, denoted as T10.

The geometry of the computational fluid dynamic (CFD) model was slightly simplified in comparison to the actual aircraft.

The 1:5 scale wind-tunnel model was based on the previously mentioned geometry for CFD. The span was reduced to fit the height of the test section. The fillets of the real geometry were retained.

The HPH304S wing employed a proprietary airfoil, the HPH_x_n2, designed for a turbulator on the lower side. In-flight testing for the optimum flap settings, evaluation of fuselage influence on the wing and the development of separation along the wingspan at high angles of attack were carried out on the first prototype, call-sign OK-0111.

Analysis methods

Three CFD codes, three wind-tunnels and three test aircraft were used for the flow analysis, with particular emphasis on transition coupled with separation bubble and both laminar and turbulent separation.

Numerical modeling

For the airfoil analysis, XFOIL[4] was used. To investigate the properties of the entire wing, the XFLR5[5] software was used.

The commercial code Fluent 6.3 was used for three-dimensional numerical simulation of wing/fuselage interaction. Turbulent flow was modeled using the k-ε turbulence model,[6] which performs well in flows involving rotation, boundary layers under strong adverse pressure gradients and separation and recirculation. Spalart-Allmaras and SST k-ω turbulence models[7,8] were assessed as well. The near-wall flow was modeled using a combination of a two-layer model and wall functions.

Wind-tunnel measurements

The closed-circuit, open test section general purpose wind tunnel, having a cross-section of 750 x 550 mm^2, of the Faculty of Mechanical Engineering, Czech Technical University in Prague was used for smoke-wire, oil flow and infrared camera visualization. The airfoil models having circular end plates were mounted horizontally (Fig. 3). The typical test Reynolds number was Re = 3.0 x 10^5 and the inlet turbulence intensity was Tu = 2.2%.

The blow-down facility of the Institute of Thermomechanics (IT), Academy of Sciences (AS) of the CR (Fig. 4) was employed for time-resolved PIV measurement at Re = 1.0 x 10^5 and Tu = 0.5%. The outlet cross-section of this facility is 250 x 250 mm^2.

The closed-circuit, closed test section, research wind-tunnel of the IT, AS, CR was used for all other tests. The test section of this facility, 865 x 485 x 900 mm,[3] was designed for airfoil and wing/body investigations.[9] Circular end plates provide an attachment for both types of models. The turntables are 500 mm in diameter and are flush with the wind-tunnel walls. They are electrically driven to enable angle of attack changes of the model. The airfoils are mounted so the center of rotation of the circular plates is at 40% of the model chord. The same fraction is preserved for the body model (Fig. 5) with respect to wing chord. The air gaps at the tunnel walls were sealed by labyrinth packing.

The typical Reynolds number of these tests was Re = 5.0 x 10^5, and the inlet turbulence intensity Tu through the whole range of velocities was 0.2%.

In-flight measurement

Standard pressure instruments and GPS-based technologies were used for data acquisition. Every measurement program was initiated at an altitude of 2000 m AGL or higher. Four individual straight flight sequences were used for each airspeed. Flight tracks of 300 m altitude-loss in each sequence were recorded. The recorded flight track was post-processed and the evaluated flight speed and sink rate were reduced to the International Standard Atmosphere.

Oil flow visualizations at several positions along the wingspan were performed on all three sailplanes. Oil was applied on the surface prior to take-off and a flight of 10 minutes duration was carried out. The airspeed was held constant during the whole flight, typically V = 100 km/h IAS, even during the climb and approach to landing.

An array of tufts was applied to the wing root area of the VSO10 and the TST10a. Video recordings were acquired by a camera located either on the tail-boom or on the fuselage top. To cover the common competition range, airspeeds V were selected ranging from 85 to 160 km/h IAS.

An integrating rake was designed (Fig. 6) and tested for drag measurement in the wind-tunnels. Later on, it was used for in-flight measurements, fixed to the flaperon of the HPH304S sailplane on wing chord c = 793 mm (Fig. 7).

Airfoils, extension to wings
The VSO10

XFOIL and XFLR5 analysis revealed laminar separation on the lower side of the upward deflected aileron on the VSO10 outer wing segment. CFD modeling with fixed transition predicted a roll-rate improvement. Lift-curve measurements confirmed this improvement by using a zig-zag

type turbulator placed at 0.03 x/c upstream aileron hinge (Fig. 8, lower branch of lift curves).

In addition, turbulent separation took place on the aileron upper surface with positive flap deflections. Vane-type rectangular vortex generators of height 3mm, with their trailing edge located 0.07 x/c upstream of the aileron hinge (Fig. 9) were used and resulted in a substantial improvement of the lift properties achieved (Fig. 8, upper branch of lift curves).

Finally, a series of test flights was flown on the VSO10C sailplane to establish influence of zig-zag type turbulator 0.03 x/c upstream of the aileron hinge. Video recordings of turn reversals from -45deg to +45deg of bank angle were taken at V = 80 km/h IAS (Fig. 10). The measured mean time for such a maneuver was 3.66 s for the clean configuration and 3.50 s when the turbulators were installed. It was found with XFLR5 that the improvement of roll-rate by passive flow control increased with decreasing airspeed. If V = 5 m/s is assumed as a critical part of initial take-off roll in aero-tow, the improvement is 2.4 times than the V = 80 km/h IAS result; sought improvement in aileron authority was achieved.

Hysteresis of the lift curve was studied on the VSO10 horizontal stabilizer that employed the NACA 64-009 airfoil with 25% chord flap. While this airfoil resulted in a penalty in available lift production when compared to the widely used Wortmann FX71-L-150/25 airfoil (HPH304C) (Fig. 11) this penalty is quite small. Although not fully recommended, the usage of thin airfoil for horizontal stabilizer is not considered dangerous with regard to cable breaks during winch launch.

The TST10

XFOIL and XFLR5 analysis (Figs. 12 and 13) demonstrated a potential of performance improvement on the TST10 by using turbulators on the lower side of the wing. This was confirmed by smoke-wire flow visualization tests showing laminar separation bubble suppression (Fig. 14). Finally, in-flight oil flow visualization was used for the identification of separation onset and reattachment (Fig. 15). It was found that the application of zig-zag turbulators along the wingspan resulted in improvements similar to those achieved on a Standard Cirrus sailplane,[10] amounting to a 10.7% improvement of overall lift-to-drag ratio.

The FX66 family of airfoils was further studied using time-resolved PIV measurements. A Dantec TR PIV system, with Pegasus Laser 2x10mJ and NanoSense Mk. III camera served for acquisition of 1635 double-images of 1280x1024 pixel resolution with a frequency of 500Hz in each test case – uncontrolled and controlled transition on the FX66-S-196V1 airfoil.

Although mean velocity fields presented in Fig. 16 indicate a separated boundary layer that corresponds well to expected behavior, showing a recirculation zone, no such flow behavior was observed in the instantaneous data. There were sequences of isolated vortices driven downstream. The full potential of the time-resolved technique should be utilized to identify the unsteady vortex structures.

The HPH304S

The possibility was studied of a drag coefficient reduction by transition control on the flapped airfoil lower surface using the flap setting for circling. Surface flow visualization and integrating rake pressure measurements for optimum transition control were taken on a high-performance sailplane, the HPH304S. No evidence of a laminar separation bubble was found on the outer part of the wing or in the transition to the winglet region. A practical application of turbulators was achieved by using a zig-zag turbulator in front of the hinge line of the flaperons. To verify the results of the calculated optimum location, oil-flow tests were flown at V = 100km/h IAS and integrating rake measurements were taken at V = 85, 100, 120 and 140 km/h IAS. The difference of mean total pressure in the wake p_m and undisturbed total pressure p_∞, p_{Rake} = p_∞ - p_m , was measured using a pressure transducer. All data were normalized using the dynamic pressure, q, such that

$$\Pi_{Rake} = p_{Rake} / q \qquad (1)$$

The calculated overall optimum location for the turbulator tape and the appropriate flap deflections for given airspeeds were confirmed experimentally. Values of Π_{Rake} for all flap deflections are presented in Fig. 17.

Wing-fuselage interaction

Since some of the effects taking place in the fuselage-wing junction[1] result in generation of vortex structures, these structures need to be identified in the flowfield. The methods used in this research were described in a recent study.[11]

The VSO10

The achievement of less altitude than expected in dolphin-style flight was the motivation for examining the suitability of the wing-fuselage fairing of the VSO10 sailplane. Steep pull-outs from V = 140 km/h IAS until stall were performed. During the entire maneuver, the flow remained attached, as can be observed in Fig. 18a. The separation appeared at only approximately 5 km/h above stall speed with the presence of buffeting. Thus, the desired aerodynamic properties were confirmed (Fig. 18b).

The TST10

CFD analysis and vortex identification were used for modeling the T10 test case geometry.[11] Generation of the horseshoe vortex was visualized, starting with a separated boundary layer on the fuselage. Also, another much smaller contra-rotating vortex was observed closer to the leading edge. More or less they follow upper and bottom surface of the wing and stretch further downstream. Wind-tunnel visualizations, carried out for five angles of attack, confirmed the formation of a separation zone in the area of interest, as shown in Fig. 19, in which the smaller inner vortex is also shown.

The HPH304S

Oil-flow visualization was carried out on the HPH304S sailplane and another typical feature of wing-fuselage geometry flow was observed. Upwash in front of the wing and downwash behind the wing were influenced by additional fuselage cross flow velocity (alpha flow) at the junction. Due to the induced angle of attack and the usually divergent shape of the junction, the location of the boundary layer transition on the wing shifted upstream closer to the junction forming a turbulent wedge. The systematic change of the airfoils towards the wing root enabled a large region of laminar flow (Fig. 20). The typical turbulent wedge was not observed.

Conclusions

Synthesis of CFD, wind-tunnel, and flight-test experiments was used for the analysis of nominally 2D and 3D boundary layers on sailplane geometries. Better insight into the flow physics was gained and several cases of flow control were studied.

Turbulators are the standard means of forcing transition on sailplanes; vortex generators are rarely used. Application of these passive flow control devices led to the improvement of both performance and handling qualities of the sailplanes examined.

The three wing-fuselage cases investigated were important test cases: minimum fairing (TST10), high angle of wing incidence (VSO10) and the combination of airfoil transition and incidence towards the fuselage (HPH304S).

Acknowledgments

References

[1] Thomas, F.: *Fundamentals of Sailplane Design*, 3rd Ed. College Park Press, 1999. 274 p. ISBN 0-9669553-0-7

[2] Althaus, D., and Wortmann, F.X., *Stuttgarter Profilkatalog I*, 1st ed., Vieweg & Sohn Verlagsgesellschaft, Braunschweig, 1981.

[3] Boermans, L.M.M. and Terleth, D.C.: Wind-tunnel Tests of Eight Sailplane Wing-Fuselage Combinations, *Technical Soaring*, Vol. 8, No. 3, 1984, pp. 70-85.

[4] Drela, M., Youngren, H.: XFOIL 6.9. MIT, 2001, 33 p., http://raphael.mit.edu/xfoil/

[5] Deperrois, A.: Analysis of foils and wings operating at low Reynolds numbers. Guidelines for XFLR5 V4.15, 2009, 53 p.

[6] Shih, T.-H., Liou, W. W., Shabbir, A., Yang, Z. and Zhu, J.: A New k-epsilon Eddy-Viscosity Model for High Reynolds Number Turbulent Flows - Model Development and Validation, *Computers Fluids*, 24(3):227-238, 1995

[7] Spalart P. and Allmaras, S.: A one-equation turbulence model for aerodynamic flows, Technical Report AIAA-92-0439, American Institute of Aeronautics and Astronautics, 1992

[8] Menter, F. R.: Two-Equation Eddy-Viscosity Turbulence Models for Engineering Applications, *AIAA Journal*, 32(8):1598-1605, August 1994

[9] Popelka, L.: Wind Tunnel Test Section for Airfoils and Bodies, Research Programme Feasibility Studies, *Proceedings of the Conference Topical Problems of Fluid Mechanics 2008*, Institute of Thermomechanics AS CR , Prague, 2008, pp. 85-88.

[10] Popelka, L.: Aerodynamic Optimization of Sailplane Airfoils, Ph.D. Dissertation, Department of Fluid Dynamics, Czech Technical University in Prague, 2006.

[11] Popelka, L., Zeleny, L., Simurda, D. and Matejka, M.: Wing-Body Interaction: Numerical simulation, Wind-tunnel and In-flight Testing, *Technical Soaring*, Vol. 34, No. 2, 2010, pp. 29-36.

[12] Maughmer, M.D., Hallman, D., Ruszkowski, R., Chappel, G., Waitz, I.: Experimental Investigation of Wing/Fuselage Interaction Geometries, *Journal of Aircraft*, Vol. 26 (1989), No. 8, p. 705-711.
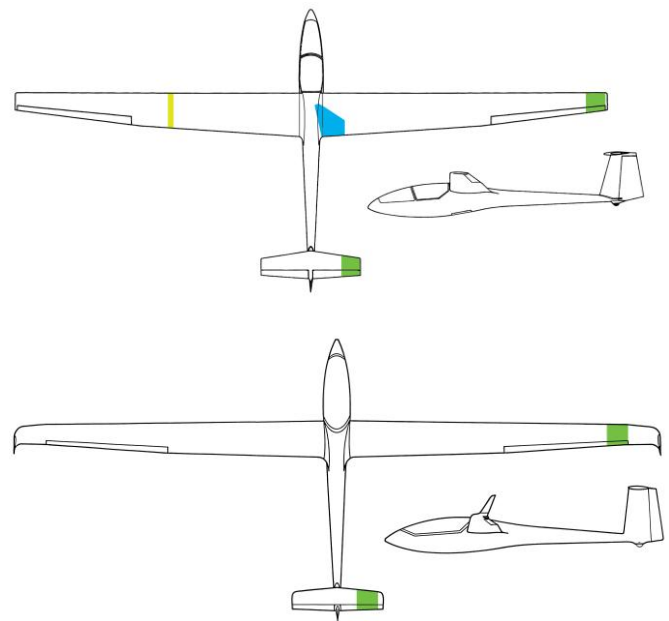
Figure 1 Club class sailplanes, the VSO10 and the HPH304C, both 15m wingspan (from top to bottom). Full-scale wind-tunnel models (green), tuft array (blue) and oil-flow pattern (yellow).
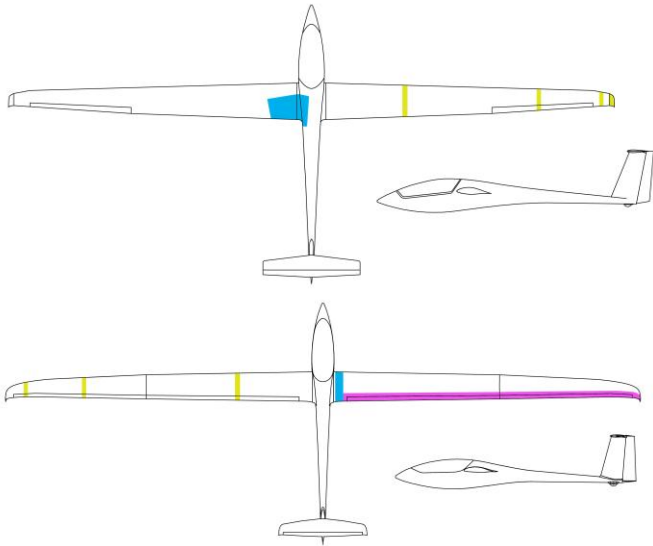
Figure 2 Self-launching sailplanes, the TST10 (15m) and the HPH304S (18m flapped) (from top to bottom). Wing-fuselage survey (blue), oil-flow pattern (yellow) and tuft array (violet).
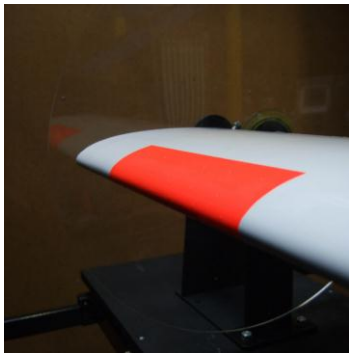
Figure 3 VSO10 wing segment with end plates with simulated strip of roughness due to insects in the 750 x 550 mm² wind-tunnel CTU in Prague.

Figure 4 Blow-down rig of 250 x 250 mm² of the IT, AS of the CR and time-resolved PIV setup with Wortmann FX66-S196V1 airfoil.

Figure 5 T10 test case geometry in the test section 865 x 485 x 900 mm³ wind-tunnel of the IT, AS of the CR with side walls removed.
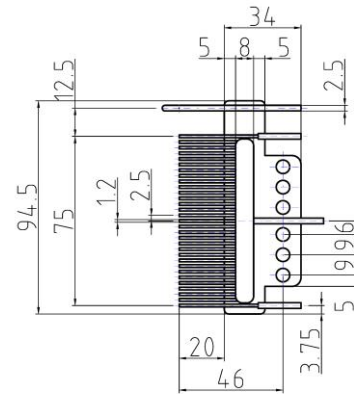
Figure 6 Integrating pressure rake for in-flight measurement.

Figure 7 Installation of pressure rake downstream the HPH304S wing trailing edge.
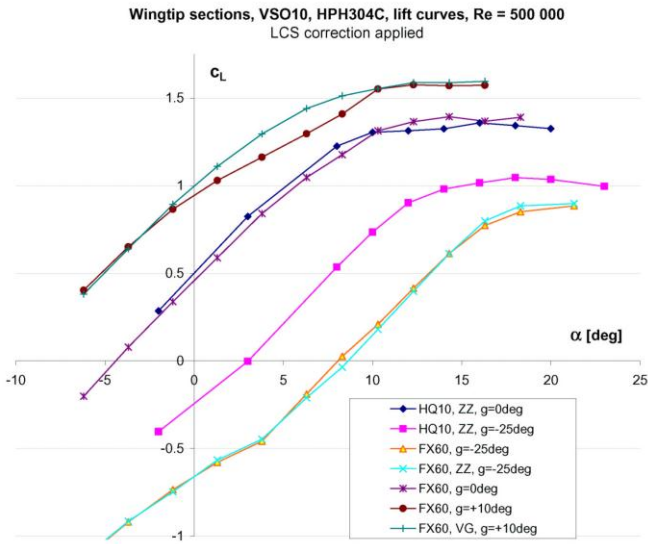
Figure 8 Comparison of lift curves from wind-tunnel measurement, Re = 5·10^5, VSO10 and HPH304C wingtip sections, effect of passive flow control devices. Flap deflections γ = -25, 0, +10deg.
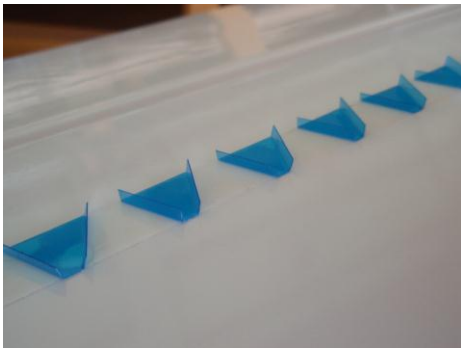
Figure 9 Vane-type vortex generators on VSO10 wing upper surface upstream aileron hinge

Figure 10 Still image from in-flight video recording, VSO10C sailplane, V = 80 km/h IAS, note lines on transparent film as a reference for turn reversal from -45 deg to +45 deg bank.
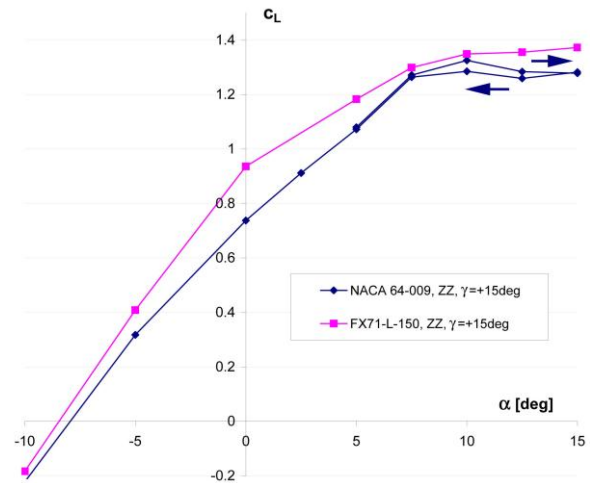
Figure 11 Comparison of lift curves from wind-tunnel measurement, Re = 5·10^5, VSO10 and HPH304C horizontal tailplane sections, effect of flow hysteresis. Flap deflection γ = +15deg.
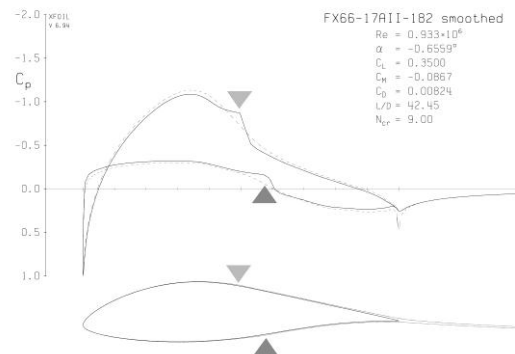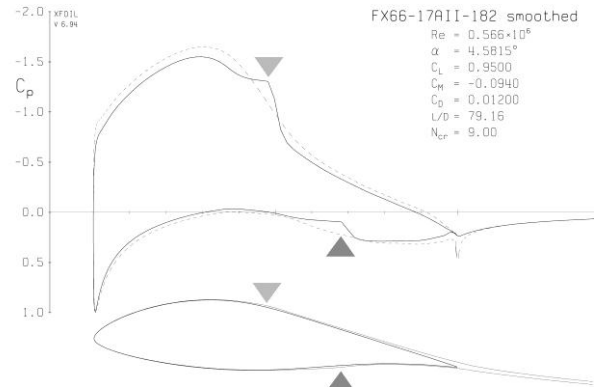
Figure 12 XFOIL analysis of TST10 wingtip airfoil for airspeeds in circling and interthermal glide, marked locations of boundary layer transition.
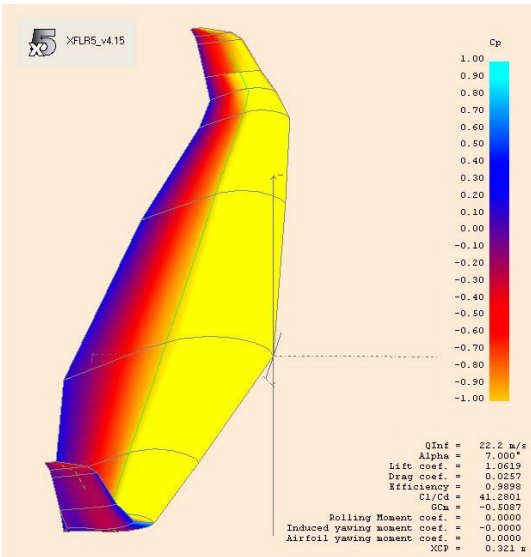
**Figure 13** XFLR5 panel method analysis of TST10a wing, $c_L = 1$, green line indicates transition.
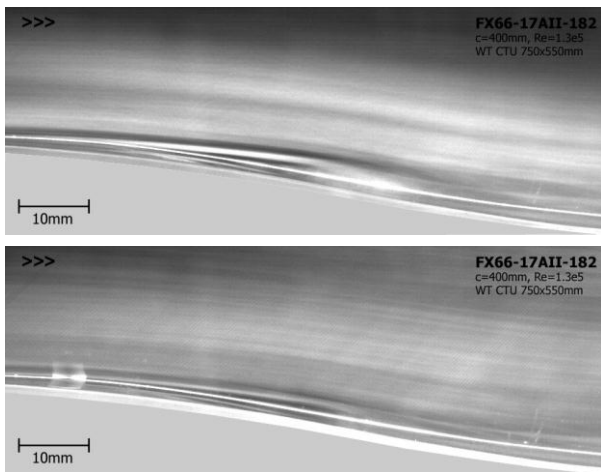

Figure 14 FX66-17AII-182 airfoil, smoke-wire visualization, bottom side, Re = $1{,}3 \cdot 10^5$, uncontrolled case (top); passive-flow control: zig-zag turbulator, $x_{Tb}/c = 0.4$.
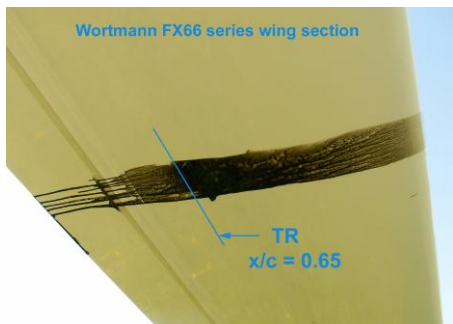

Figure 15 Oil-flow visualization on lower surface of outer wing segment of TST10a sailplane, in the aileron region. Local chord c = 490 mm, V = 100 km/h IAS. Right to left: laminar boundary layer, separation bubble, turbulent boundary layer; TR − turbulent reattachment line.
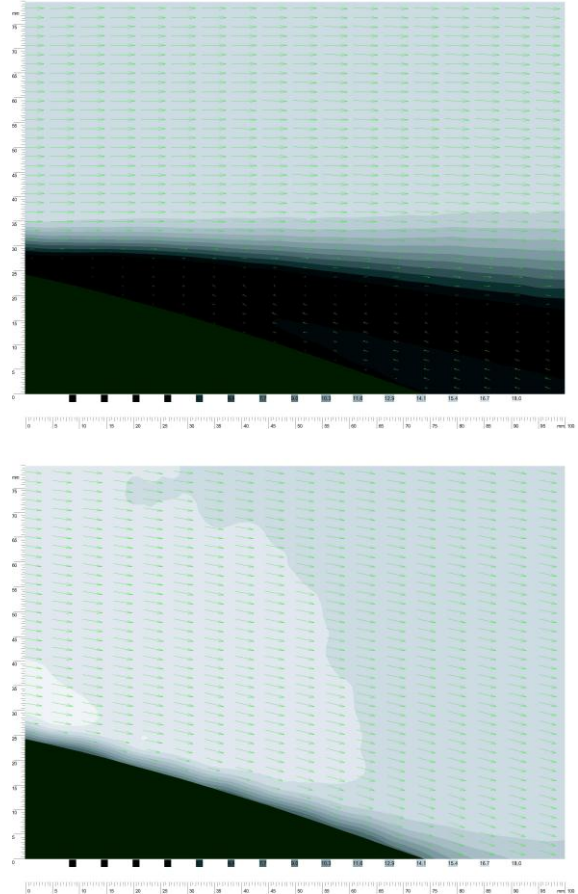

Figure 16 FX66-S-196V1 airfoil, TR PIV mean velocity field, top side, Re = 10^5, uncontrolled case (top); passive-flow control: zig-zag turbulator, $x_{Tt}/c = 0.1$ (bottom).
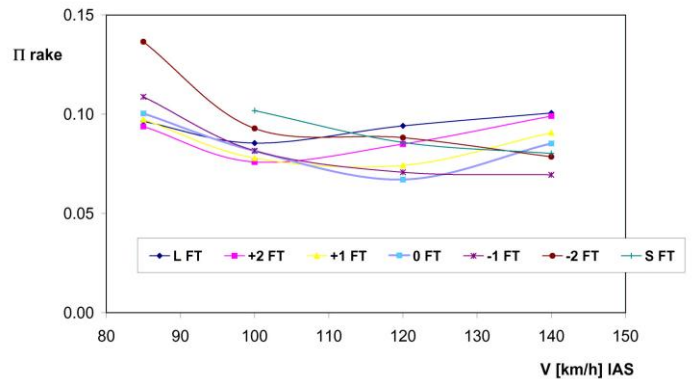

Figure 17 Normalized integrating rake pressure difference ΠRake. The HPH304S sailplane and the HPH_x_n2 airfoil, chord c = 793 mm, factory installed turbulators (FT configuration).

Figure 18 VSO10C sailplane, wing root tuft visualization, V = 140 km/h IAS, attached flow (top); V = 70 km/h IAS, bank angle 30 deg, stalled flow (bottom).
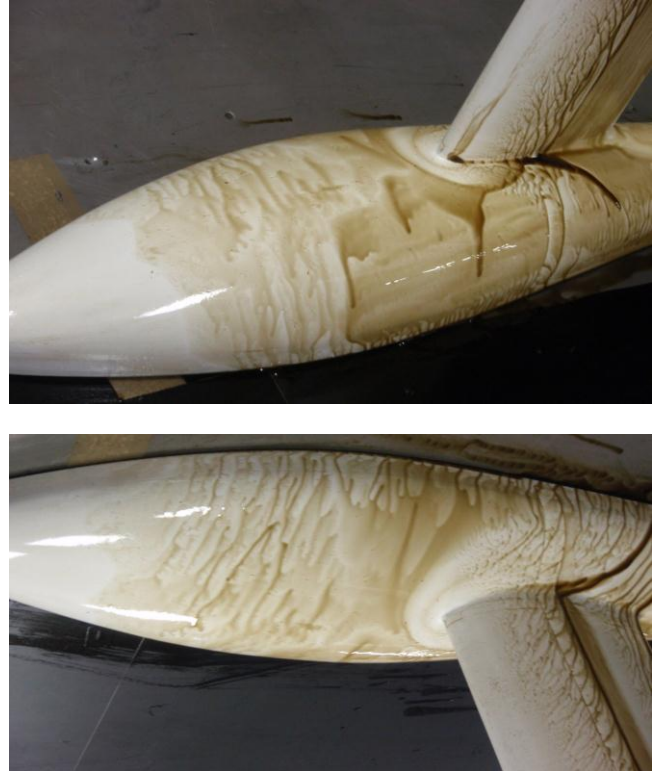
Figure 19 Oil-flow visualization in 750 x 550 mm^2 wind tunnel test section on T10 test case 1:5 scale model, Re_c = 2.0 x 10^5, α = - 5deg.
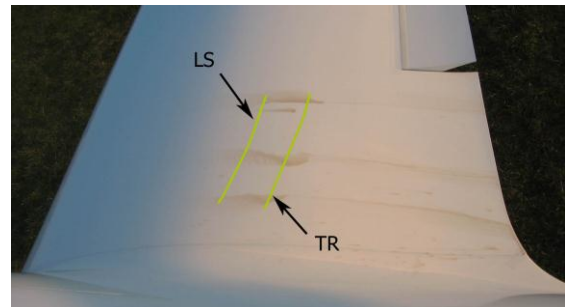

Figure 20 The HPH304S sailplane, wing root oil flow visualization, V = 100 km/h IAS, natural laminar separation (LS) and turbulent reattachment (TR).